A COMPARISON BETWEEN THE PRESENCE AND ABSENCE OF VIRTUAL VISCOSITY IN THE BEHAVIOUR OF THE TWO PHASE FLOW INTERFACE

by

Iman ABBASPOUR, Vahid SHOKRI*, and Morteza ABBASI

Department of Mechanical Engineering, Sari Branch, Islamic Azad University, Sari, Iran

Original scientific paper
https://doi.org/10.2298/TSCI200801163A

In this paper, a numerical study is performed in order to investigate the effect of the virtual viscosity on simulation of separated two-phase flow of gas-liquid. The governing equations solved by shock capturing method which can provide predicting the interface without the flow field solving. In this work, in order to calculate the numerical flux term, first-order centered scheme (Force scheme) was applied cause of its accuracy and appropriate validation. Analysis approves that the obtained stability range of this research is consistent with the classic Kelvin-Helmholtz instability equation only for the long wavelength with small amplitude. Results reveal that when the wavelengths are reduced, the specified range is not consistent and wavelength effects on instability range and it is overpredicted. An algorithm for water faucet problem was developed in FORTRAN language. Short wavelength perturbations induce unbounded growth rates and make it impossible to achieve converging solutions. The approach taken in this article has been to adding virtual viscosity as a CFD technique, is used to remedy this deficiency.

Key words: *multiphase flow, two phase flow, two-fluid model, numerical simulation, virtual viscosity*

Introduction

Two-phase flow of gas and liquid is simultaneous transmission of gas and liquid in an internal flow like a pipe or channel [1]. Choosing the optimal mathematical model according to the limitations of available models is a fundamental challenge to predict flow dynamics [2, 3]. Because of the existence of the shape changeable interface and compressibility of the gas phase, separated two-phase flow of gas-liquid modeling is complicated [4]. This deformability causes the fluid properties to change in passing the interface discontinuously. In these problems, shock interactions that accounted as a discontinuity in fluid properties, and interface as another discontinuity cause afflictions in simulating and instabilities capturing in the interface [5, 6]. There are two different types of formulations called mixed fluid model and separated two-fluid model [1, 7]. Mixed fluid model consists of a dispersed phase and a continuous phase. Mixed fluid models such as homogeneous equilibrium model (HEM) and drift flux model (DFM) are involved with fewer equations and describe the properties of mixtures such as momentum or energy [7]. This model is convenient for flows that phases are coupled strongly and the relative velocity between the phases is negligible [5]. The DFM compared to the HEM, the velocity difference between the phases is taken into account [8]. The second

* Corresponding author, e-mail: shokri.vhd@iausari.ac.ir

formulation is the separated two-fluid model in which based on two types of conservation equations for each phase. In general, each phase has its own pressure, velocity, and temperature [9]. The two-fluid model is more suited for flows that phases are coupled together weakly and wave propagates in each phase at different velocities [9, 10]. This study has applicated and focused on two-fluid model as a desirable and comprehensive model. The 1-D form of this model was obtained from surface integration (area averaging) of the 3-D equations of fluid properties over a cross section of the flow [11]. Momentum transmission between the fluids and pipe wall, and also dynamic interactions of phases at the interface, is indicated as a source term and obtained from empirical relations [11, 12]. Various forms of two-fluid model have been developed according to the performance of phase pressures: pressure free model (PFM) that the pressure does not appear in the equations, single pressure model (SPM) which both of the phase pressures are equal, and two pressure model (TPM) that the phase pressures are different [6, 13-15].

A physical model should provide flow pattern predicting, limitations, and uncertainties in the flow properties with precise numerical methods [16]. Widely researches have done in order to find an accepted criterion for the well-posedness of two fluid models [17]. A review of previous researches shows that two-fluid models are sensitive to the roots of the characteristic equation [7, 18]. The TPM is always hyperbolic and PFM and SPM are hyperbolic within a specified range [9, 11, 19]. One of the features of the TPM and SPM is the non-conservative aspect of its governing equations and an additional method must be introduced for non-conservative term. The PFM equations are conservative but in order to determine well-posed range of the model, a hyperbolic analysis is required [20]. Hyperbolic analysis shows that ill-posedness is related to the unbounded growth of short wavelength perturbations [11, 21]. Surface tension which appears as a source term in the governing equations introduces a cut-off wavelength. This is suitable for short wavelengths and on the contrary with long wavelength assumptions because of the wavelengths above the cut-off, experience illogical high growth rates [22]. The grid diffusivity was used to annihilate the growth of short wavelengths but the grid independence verification was not achieved for all the conditions [11].

Previous works reveal that when the wavelengths are reduced, the specified district is not consistent and wavelength effects on stability range and it is overpredicted [2, 10, 21]. In the present work an algorithm for water faucet problem which is a famous problem in multiphase flows, was developed and implemented in FORTRAN code. Short wavelength perturbations induce unbounded growth rates and make it impossible to achieve converging solutions. The approach taken in this article has been to adding virtual viscosity as a CFD technique, is used to remedy this deficiency. Virtual viscosity is introduced to damp the unbounded growth of instabilities where the standard model is not well-posed. The present study aims to explore the possibility of mathematical regularization of a virtual viscosity in the governing equations. According to the non-physical nature of these instabilities, it seems that a mathematical approach can lead to a convergent solution. A comparison of the numerical results with analytical results is done on a benchmark problem and it is showing a good agreement.

Mathematical models

In this paper, the SPM and the free pressure model have been chosen as the physical models. The present study is based on the transport equations for an isothermal flow and therefore consists of conservation of mass and momentum for the gas and liquid. Figure 1 illustrates the schematic of the separated two phase flow in a pipe. The a_k and u_k are cross-section area, and velocity. The s_i and s_k are wetted perimeters of interface and each phase. The

τ_i and τ_k are the interface and phase-wall shear stresses, respectively (k = l, g, and i is defined as the liquid, gas, and interface notations). The h_l and A are liquid height, and area of the whole cross section of the pipe.

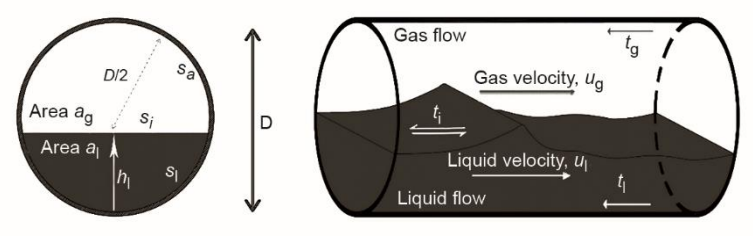

Figure 1. Schematic of the separated two phase flow of gas and liquid

Single pressure model

The governing equations on the SPM are included two series of continuity and momentum equations. Mass conservation equation:

$$\partial_t(\rho_k\alpha_k) + \partial_x(\rho_k\alpha_k u_k) = 0 \tag{1}$$

Momentum conservation equation:

$$\partial_t(\rho_k\alpha_k u_k) + \partial_x(\rho_k\alpha_k u_k^2 + \alpha_k P) = P_i\partial_x(\alpha_k) - \alpha_k\rho_k \mathrm{G}\sin\theta_k - \tau_k s_k A^{-1} \mp \tau_i s_i A^{-1} \tag{2}$$

where ρ_k, a_k, and u_k are density, cross-section area, and velocity (k = l, g, and i is defined as the liquid, gas, and interface notations), respectively, s_i and s_k – the wetted perimeters of interface and each phase, P and P_i – the phase and interface pressure, τ_i and τ_k – the interface and phase-wall shear stresses, respectively, G – the gravitational acceleration, h_l – the liquid height, θ – the pipe inclination (is required for inclined pipe), and A – the area of the whole cross section of the pipe (gas and liquid). In the SPM, the pressure of both phases is equal as well as the pressure of phases at the interface are the same. The + and – of the $\tau_I S_I A^{-1}$ is identified according to the flow direction as shown in fig. 1

Free pressure model

Free pressure model consists of a hybrid mass and a hybrid momentum equation. Hybrid mass conservation equation is obtained from summation of gas and liquid mass equations with the incompressibility assumption of the gas and liquid phases.

Hybrid continuity equation:

$$\partial_t(\rho_l\alpha_l + \rho_g\alpha_g) + \partial_x(\rho_l\alpha_l u_l + \rho_g\alpha_g u_g) = 0 \tag{3}$$

Hybrid momentum conservation equation is obtained from mixing (some mathematical operations) of gas and liquid momentum equations of the SPM:

$$\begin{aligned}\partial_t(\rho_l u_l - \rho_g u_g) + \partial_x(0.5\rho_l u_l^2 - 0.5\rho_g u_g^2 + \Delta\rho \mathrm{G}\cos\theta h_l) = \\ = -\Delta\rho \mathrm{G}\sin\theta + (a_l^{-1} + a_g^{-1})\tau_i s_i + \tau_g s_g a_g^{-1} - \tau_l s_l a_l^{-1}\end{aligned} \tag{4}$$

where α_l, α_g, u_g, and u_l are unknowns in the FPM equations system. To find the primitive unknowns, eqs. (3) and (4) must be supplemented at least by two more equations. Since the flu-

ids are assumed incompressible, algebraic constraint $C(t)$, which is a known function of time dependent on the inlet boundary flow parameters is obtained [11, 16]:

$$\partial_x(\alpha_\mathrm{l}u_\mathrm{l}+\alpha_\mathrm{g}u_\mathrm{g})=0\rightarrow\alpha_\mathrm{l}u_\mathrm{l}+\alpha_\mathrm{g}u_\mathrm{g}=C(t)=(\alpha_\mathrm{l}u_\mathrm{l}+\alpha_\mathrm{g}u_\mathrm{g})_\mathrm{inlet} \tag{5}$$

Another relation is obtained from the geometric constraint:

$$a_\mathrm{l}+a_\mathrm{g}=A\rightarrow\ \alpha_\mathrm{g}=a_\mathrm{g}A^{-1},\quad \alpha_\mathrm{l}=a_\mathrm{l}A^{-1},\quad \alpha_\mathrm{g}+\alpha_\mathrm{l}=1 \tag{6}$$

Shear stress

The shear stresses are illustrated in fig. 1 are comprised of wall-phase shear stresses and shear stress at the interface of gas and liquid. Distribution of them on the pipe wall has a vital role in determining the turbulence structure inside the pipe as well as the flow resistance [22, 23]:

$$\tau_k=0.5\ f_k\rho_k u_k|u_k|$$

$$\tau_i=0.5\ f_i\rho_\mathrm{g}u_\mathrm{g}\Delta u|\Delta u| \tag{7}$$

where f_k and f_i represent phases and interface friction factors, respectively:

$$f_k=\max(16\,\mathrm{Re}_k^{-1},0.046\,\mathrm{Re}_k^{-0.2})$$

$$f_i=f_\mathrm{g} \tag{8}$$

in which hydraulic diameter $D_{\mathrm{h}k}$ is applied for calculation of Reynolds number Re_k in each phase instead of inner diameter:

$$\mathrm{Re}_k=\rho_k D_{\mathrm{h}k}|u_k|\mu_\mathrm{l}^{-1},\quad D_\mathrm{hl}=4a_\mathrm{l}s_\mathrm{l}^{-1},\quad D_\mathrm{hg}=4a_\mathrm{g}(s_\mathrm{g}+s_\mathrm{l})^{-1} \tag{9}$$

Geometric variables appearing to calculate the wetted perimeter of each phase can be found from previous works [18, 24].

Hyperbolic analysis

The present study does not intend to scrutinize the attainment methodologies of hyperbolic analysis and their validation. But the result of the present approach will affect the analysis and improve its stability range. Therefore, only the final results of the models used in this study are to be expressed.

In general, there are two kinds of hyperbolic analysis methods depending on the presence/absence of conservative term in the governing equations [18]. To determine the stability range of interface waves, various relations are offered that based on classic Kelvin-Helmholtz relation [10, 19, 25]. The SPM and PFM are sensitive depending on whether the characteristic values of governing equations are real or complex [11, 18]. Previous studies demonstrated these challenges directly related to the velocity difference between the phases:

$$u_\mathrm{g}-u_\mathrm{l}\le K\sqrt{(\alpha_\mathrm{g}\rho_\mathrm{l}+\alpha_\mathrm{l}\rho_\mathrm{g})\frac{\Delta\rho}{\rho_\mathrm{l}\rho_\mathrm{g}}\mathrm{G}\cos\theta\frac{a}{\dfrac{\mathrm{d}a_\mathrm{l}}{\mathrm{d}h_\mathrm{l}}}} \tag{10}$$

where ρ_k, a_k, α_k, and u_k are density, cross-section area, phase volume fraction, and velocity ($k = l, g$ is defined as the liquid, and gas), respectively, G – the gravitational acceleration,

h_l – the liquid height, θ – the pipe inclination, and a – the area of the whole cross-section of the pipe. If the relationship (10) is not satisfied, the roots of the characteristic equation are imagined and the model is ill-posed and the interface is physically unstable as well. It means that limit of physical instability at the interface is equal to well-posing of model. Ill-posing causes that the results do not show realistic physics. In the above equation, coefficient, *K*, for the inviscid assumption is one, and for the viscous assumption *K* is obtained from results of previous works [11, 26]:

$$K = \sqrt{1 - \frac{(C_V - C_{IV})^2}{\dfrac{\Delta\rho}{\dfrac{\rho_l}{\alpha_l} - \dfrac{\rho_g}{\alpha_g}} G\cos\theta \dfrac{a}{\dfrac{da_l}{dh_l}}}} \tag{11}$$

where C_{IV} and C_V are critical wave velocities from the inviscid and viscous stability analyses, respectively, which is obtained from the equation suggested by the Barnea and Taitel [19].

Virtual viscosity

In the CFD, the words *numerical dissipation/dispersion* and *virtual viscosity* are frequently used interchangeably and generally connote the diffusive behavior (which is purely numerical in origin) of a numerical solution. Numerical dissipation is a direct result of the even-order derivatives and numerical dispersion is a result of the odd-order derivatives of the governing equations [27, 28]. Although virtual viscosity decreases the accuracy of a solution, on the contrary, it increases the stability. Indeed, for many flow problems with strong gradients, such as shock waves, where shocks are captured within the flow by using a shock capturing method, addition of virtual viscosity is an appropriate approach to achieve a stable and smooth solution, whereas without it, no solution would be attainable [27, 29]. Virtual viscosity which is the result of even-order derivative terms in the Taylor expansion, reduces strong gradients in the solution field and provides a convenient termination to the existing model in the short wavelength limit. In the present study, the matrix ε is added to the original equations as virtual viscosity.

Numerical calculation methods

The transport equations which were mentioned in section *Mathematical models* can be rewritten in a compact generic form:

$$\partial_t(\Phi) + \partial_x[\Psi(\Phi)] - \zeta\partial_x(\Phi) = \xi(\Phi) \tag{12}$$

where Φ, ξ, and Ψ are, vector field of conservative variables, vector including all source terms, and conservative flux vector, respectively. The $\zeta\partial_x(\Phi)$ contains all the non-conservative terms which present in the selected model. It is obvious that ζ determines the being conservative of the model:

Generic form for SPM:

$$\upsilon(\alpha_l, u_l, u_g, \rho_g) = (\alpha_l u_g, u_l, \rho_g)^T$$

$$\Psi(\Phi) = [\rho_g\alpha_g u_g \quad \rho_l\alpha_l u_l \quad \rho_g\alpha_g u_g^2 + \alpha_g P \quad \rho_l\alpha_l u_l^2 + \alpha_l P]^T$$

$$\Phi(\upsilon) = [\rho_g\alpha_g \quad \rho_l\alpha_l \quad \rho_g\alpha_g u_g \quad \rho_l\alpha_l u_l]^T$$

$$\xi(\Phi)=\begin{bmatrix}0 & 0 & -\rho_g\alpha_g G\sin\theta-\tau_i s_i A^{-1}-\tau_g s_g A^{-1} & -\rho_l\alpha_l G\sin\theta+\tau_i s_i A^{-1}-\tau_g s_g A^{-1}\end{bmatrix}^T \tag{13}$$

$$\zeta=\begin{bmatrix}0 & 0 & 0 & 0\\ 0 & 0 & 0 & 0\\ 0 & P/\rho_l & 0 & 0\\ 0 & P-(P/\rho_l) & 0 & 0\end{bmatrix}$$

where υ and ζ are the vector of unknowns of the model and coefficient matrix of the non--conservative vector, respectively. And also, generic form of PFM:

$$\upsilon(\alpha_l,u_l)=\begin{bmatrix}\alpha_l & u_l\end{bmatrix}^T$$

$$\Psi(\Phi)=\begin{bmatrix}\rho_l\alpha_l u_l+\rho_g\alpha_g u_g & 0.5\rho_l u_l^2-0.5\rho_g u_g^2+\Delta\rho G\cos\theta h_l\end{bmatrix}^T$$

$$\Phi(\upsilon)=\begin{bmatrix}\rho_l\alpha_l+\rho_g\alpha_g & \rho_l u_l-\rho_g u_g\end{bmatrix}^T \tag{14}$$

$$\xi(\Phi)=\begin{bmatrix}0 & -\Delta\rho G\sin\theta+(a_l^{-1}+a_g^{-1})\tau_i s_i+\tau_g s_g a_g^{-1}-\tau_l s_l a_l^{-1}\end{bmatrix}^T$$

$$\zeta=0$$

Discretization

By applying the shock capturing method algorithm to discretize the generic form, a forward approximation is used for time derivative and central approximation is used for the local derivative Toro [30]:

$$\Phi_j^{n+1}=\Phi_j^n+\Gamma(\Psi_{j-1/2}^n-\Psi_{j+1/2}^n)+\Delta t\zeta\partial_x(\Phi)+\Delta t\,\xi_j,\quad \Gamma=\frac{\Delta t}{\Delta x} \tag{15}$$

where n, $n+1$, Δt, and Δx are the old time and new time values, time step, and mesh size, respectively and j denotes cell position. The $\Psi_{j+1/2}^n$ is a numerical flux that is an approximation of physical flux. Depending on the scheme that has been chosen for $\Psi_{j+1/2}^n$, various Riemann numerical solvers are achieved. In order to calculate the numerical flux term, first-order centred scheme (Force) was used. In this method, the flux term is calculated as following [7, 30]:

$$\Psi_{j+1/2}^{\mathrm{FORCE}}=0.5(\Psi_{j+1/2}^{\mathrm{LF}}+\Psi_{j+1/2}^{\mathrm{RI}}) \tag{16}$$

where $\Psi_{j+1/2}^{\mathrm{LF}}$ and $\Psi_{j+1/2}^{\mathrm{RI}}$ are Lax-Friedrichs and Richtmyer methods. Richtmyer and Lax--Friedrichs never used for practical applications. Richtmyer is dispersive and induces numerical spurious waves, and Lax-Friedrichs is diffusive and will damp most flow features [4]. Toro proposed a new first-order centered method to avoid the bad effects of Richtmyer and Lax-Friedrichs methods. In Force method the intercell flux is an arithmetic mean of the Richtmyer and Lax-Friedrichs fluxes [30, 31]. Lax-Friedrichs method is a first-order scheme in time and space and numerical flux term is calculated by:

$$\Psi_{j+1/2}^{\mathrm{LF}}=0.5(\Psi_{j+1}^n+\Psi_j^n)-0.5\Gamma^{-1}(\Phi_{j+1}^n-\Phi_j^n) \tag{17}$$

Richtmyer method is an explicit and second-order in time and space which calculated in two steps:

$$\Phi_{j+1/2}^{n} = 0.5(\Phi_{j}^{n} + \Phi_{j+1}^{n})$$

$$\bar{\Phi}_{j+1/2} = \Phi_{j+1/2}^{n} - 0.5\Gamma(\Psi_{j+1}^{n} - \Psi_{j}^{n}) + 0.5\Delta t\xi(\Phi_{j+1/2}^{n})$$

$$\Psi_{j+1/2}^{\mathrm{RI}} = \Psi(\bar{\Phi}_{j+1/2}) \tag{18}$$

In order to discretize the non-conservative term in eq. (12) (for SPM, particularly) a second order upwind discretization is used [7]:

$$\zeta\partial_x(\Phi) = \frac{\zeta_j^n}{\Delta x}\min \mathrm{mod}[2(\Phi_{j+1}^{n} - \Phi_{j}^{n}), 0.5(\Phi_{j+1}^{n} - \Phi_{j-1}^{n}), 2(\Phi_{j}^{n} - \Phi_{j-1}^{n})] \tag{19}$$

The min-mod-2 in eq. (1) is defined:

$$\min \mathrm{mod}(x, y, z) = \begin{cases} S.\min(|x|, |y|, |z|) & \text{if } \operatorname{sign}(x) = \operatorname{sign}(y) = \operatorname{sign}(z) \\ 0 & \text{othewise} \end{cases} \tag{20}$$

As discussed in the previous section, the present study focuses on the implementation of virtual viscosity to regulate instabilities. Simulation results in the next section demonstrate that free pressure model is more convenient to use than the SPM, in terms of process time and implementation of numerical method in the benchmark problem. But this model still has spurious oscillations where severe gradients are founded. To solve this deviance, matrix ε is coupled with the original transport equation as a coefficient for second order derivative:

$$\partial_t(\Phi) + \partial_x[\Psi(\Phi)] - \varepsilon\partial_\upsilon(\Phi)\partial_{xx}(\upsilon) = \xi(\Phi) \tag{21}$$

In fact, this is eq. (12) with a second order tensor has been added. But for the newly added part of the equation, a new method must be used. Non-conservative second order tensor of $\varepsilon\partial_\upsilon(\Phi)\partial_{xx}(\upsilon)$ complicates the solution which cannot be solved by the methods mentioned above. In the present study, equations are solved using an alternating two-step mathematical technique which consists of an implicit and a finite volume method that are coupled together strongly [32].

Step one: solving diffusion part of eq. (21) by an implicit method:

$$\partial_t(\upsilon) = \varepsilon\partial_{xx}(\upsilon) \tag{22}$$

where it can be solved by using an implicit method like Crank-Nicholson in step one such as [28]:

$$\frac{\upsilon_j^{n+1} - \upsilon_j^n}{\Delta t} = 0.5\frac{\varepsilon}{(\Delta x)^2}[(\upsilon_{j+1}^{n+1} - 2\upsilon_j^{n+1} + \upsilon_{j-1}^{n+1}) + (\upsilon_{j+1}^{n} - 2\upsilon_j^{n} + \upsilon_{j-1}^{n})] \tag{23}$$

Variables are calculated by integration on the first half-time at time step *n*. The output data of this step is used as the input data of step two.

Step two: solving advection-source term part of eq. (31) by an explicit method in step two:

$$\partial_t(\Phi) + \partial_x[\Psi(\Phi)] = \xi(\Phi) \tag{24}$$

Updated variables are calculated by integration on the full-time step and output data of this step is used as the input data of step one but on the last half-time step at time step *n*. This alternating technique is a semi-implicit method and the time step must be controlled to achieve convergence results.

Time step and boundary conditions

The first step is an implicit method then is always stable. But the second step is explicit and the size of the time step needs to be controlled by [33]:

$$(\Delta t)^n = \mathrm{CFL}\frac{\Delta x}{\lambda_{c,\max}^n} \tag{25}$$

where Δt, Δx, and CFL are the time step, mesh size, and Courante-Friedrichs-Levy number. In order to calculate time step in this paper, value of the Courante-Friedrichs-Levy number is assumed 0.5 and $\lambda_{c,\max}^n$ is the maximum eigenvalue of the Jacobian of the eq. (25) which is equal to:

$$\lambda_{c,\max}^n = \max_j\left\{\max_j\left|\lambda_j^k\right|\right\} \text{ for } j = 1,2,\ldots,M \quad k = 1,\mathrm{Neq} \tag{26}$$

where λ_j^k is wave velocity in each computational cell [18]. The schematic of the computing domain of an internal flow can be illustrated by fig. 2. Domain is discretized into M cells and special conditions are at the boundary positions $x = 0$ and $x = L$, where provide numerical fluxes $\Psi_{0.5}$ and $\Psi_{M+0.5}$ to advance the extreme cells 1 and M to the next time level in eq. (15). For this purpose, an artificial grid will be considered at the input and output, and zeroth-order extrapolation for the virtual points will be used for the flux in entry and outlet which denoted 0 and M + 1.

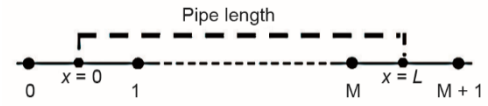

Figure 2. Schematic of the computational domain of an internal flow

Results and discussion

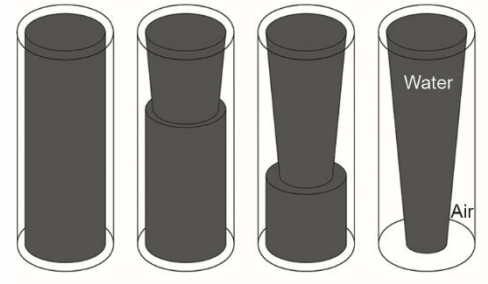

Figure 3. Schematic of the water faucet problem

In this section, the results of the simulation case are presented to demonstrate the conclusions discussed. The aim is to substantiate that the addition of virtual viscosity renders it possible to have converging numerical solutions consistent with the long wavelength assumption also for flow conditions outside the classic Kelvin-Helmholtz criteria. For this purpose, the water faucet problem is used as a benchmark case to test the role of virtual viscosity in the well-posedness of two fluid models and stability analysis. The schematic of the water faucet problem is illustrated in fig. 3 which comprised of a free fall of a column of water in a pipe where has a height of 12 meters and a diameter of 1 meter. At time $t = 0$ the velocity of water

is 10 m/s, velocity of air is 0 m/s, and the volume fraction of water is assumed 0.8. The pressure in the pipe is equal to 10^5 Pas. Inlet conditions is equal to the initial values and for outlet of the pipe a fully developed condition is assumed. Density of air is 1.16 kg/^{m3} and density of water is considered 1000 kg/m^3. In order to validate modeling accuracy, numerical method mentioned in the previous section is used for simulation and the results are compared with the analytical solution. Then the virtual viscosity is added and will investigate its effects on the well-posedness.

Analytical solution

Analytic solution of water faucet problem is extracted from Evje and Flatten [34]:

$$\alpha_{\mathrm{l}}(x,t)=\begin{cases}\dfrac{\alpha_{\mathrm{l}}^{\mathrm{inlet}}u_{\mathrm{l}}^{\mathrm{inlet}}}{\sqrt{(u_{\mathrm{l}}^{\mathrm{inlet}})^2+2\mathrm{G}x}} & x\le u_{\mathrm{l}}^{\mathrm{inlet}}t+0.5\mathrm{G}t^2\\ \alpha_{\mathrm{l}}^{\mathrm{inlet}} & x>u_{\mathrm{l}}^{\mathrm{inlet}}t+0.5\mathrm{G}t^2\end{cases}$$

$$\alpha_{\mathrm{g}}(x,t)=1-\alpha_{\mathrm{l}}(x,t)$$

$$u_{\mathrm{l}}(x,t)=\begin{cases}\sqrt{(u_{\mathrm{l}}^{\mathrm{inlet}})^2+2\mathrm{G}x} & x\le u_{\mathrm{l}}^{\mathrm{inlet}}t+0.5\mathrm{G}t^2\\ u_{\mathrm{l}}^{\mathrm{inlet}}+\mathrm{G}t & x>u_{\mathrm{l}}^{\mathrm{inlet}}t+0.5\mathrm{G}t^2\end{cases} \tag{27}$$

where α_i, u_i, and t are liquid volume fraction, liquid velocity, and time respectively. The axial coordinate is x, gravitational acceleration is G and superscript *inlet* is inlet notation of flow.

Simulation results

As pointed out earlier, we chose to present the results referring to two different types of two fluid models: SPM and PFM. All the simulations and algorithms are implemented in FORTRAN language and results are compared with the analytical solution. Figures 4 and 5 show the liquid volume fraction and liquid velocity for different computational cells 100, 200,

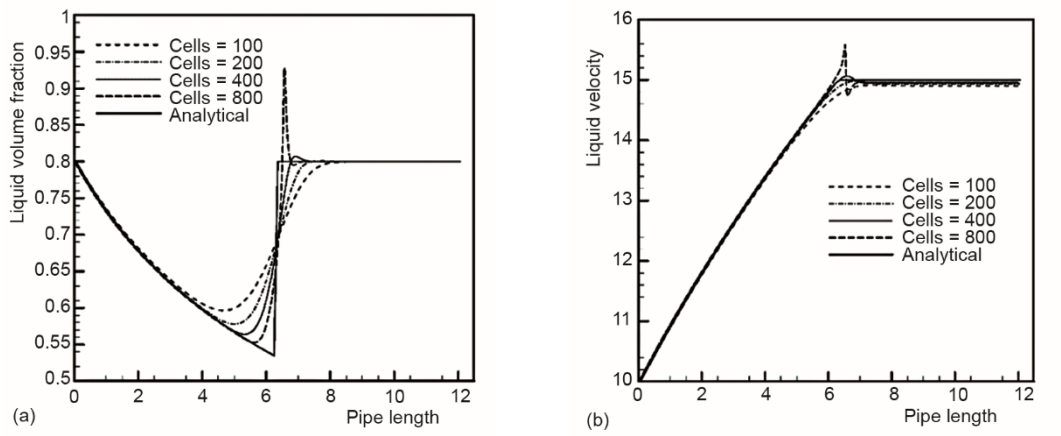

Figure 4. Water faucet problem (CFL = 0.5, computational time = 0.5 seconds); mesh refinement for (a) liquid volume fraction and (b) liquid velocity [ms^{-1}], using the Force method (PFM)

400, and 800 using analytical solution and Force method. Figure 4 is based on PFM and fig. 5 is based on SPM. The first step in assessing the quality of simulation is the independence of the computational cells and its convergence. Figure 6 shows diagrams of comparison of PFM, SPM, and analytical methods for computational cells 800. Although SPM Force method does not show dispersive behavior under the same conditions, but it has dissipative behavior in points wherein such strong gradients such as shock wave is existing. The processing time is another important criterion in any simulation and it is obvious that a conservative form of a model takes less time than a non-conservative. According to the results and argument stated above PFM Force method is the best method for modeling this case study but to improve and eliminate its defection, a new solution must be found. Figure 7 indicates effects of adding virtual viscosity to the original equations for water faucet problem for computational cells 850. Comparative diagrams is clearly indicating the effect of presence and absence of virtual viscosity in the conservation equations. From fig. 7, it is evident that the simulation with virtual

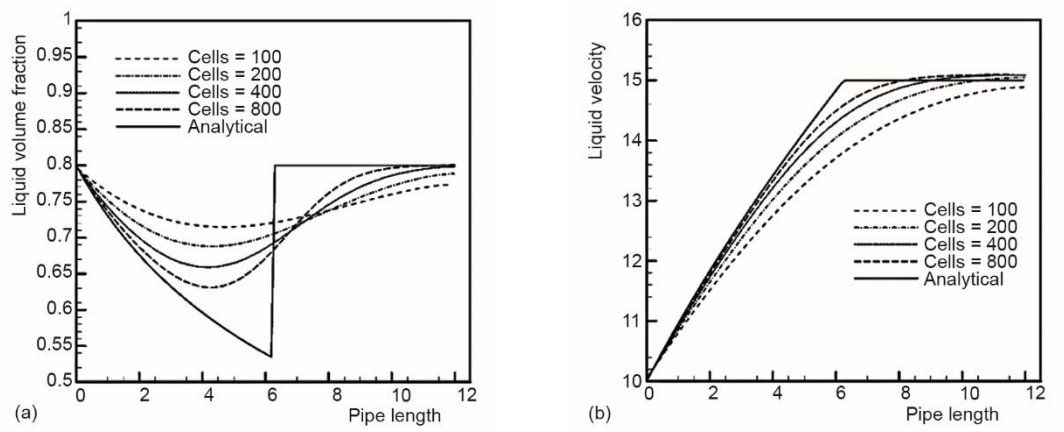

Figure 5. Water faucet problem (CFL = 0.5, computational time = 0.5 seconds); mesh refinement for (a) liquid volume fraction and (b) liquid velocity [ms^{-1}], using the Force method (SPM)

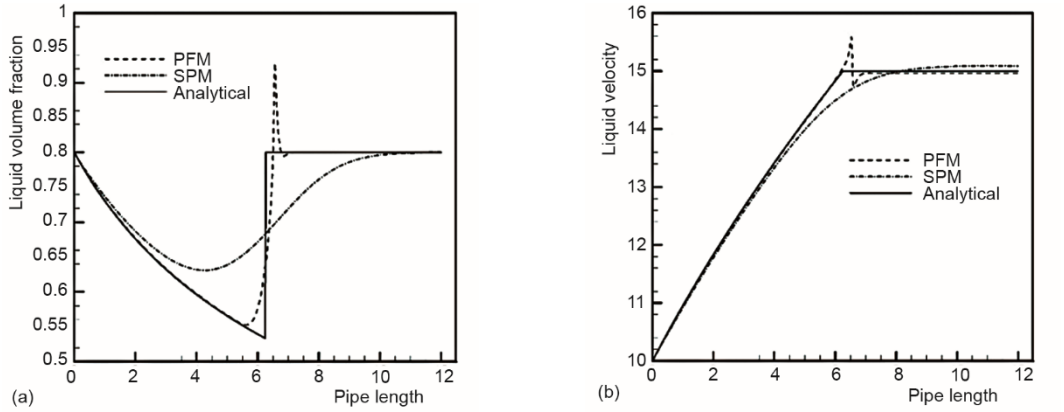

Figure 6. Water faucet problem (CFL = 0.5, computational time = 0.5 seconds); comparison of PFM, SPM, and analytical methods for computational cells 800; (a) liquid volume fraction and (b) liquid velocity [ms^{-1}]

viscosity provides converging solutions as the grid is refined. In fig. 8, the liquid volume fraction profiles are plotted for a selection of grid sizes for the simulations with and without virtual viscosity. For the simulation containing virtual viscosity, the short wavelength perturbations have damped while the larger wave grows softly and goes downstream. On the other hand, for the simulation without virtual viscosity, the short wavelength disturbances have grown severely and create high-frequency and high-amplitude oscillations in the solution field, and therefore make it an ill-posed problem.

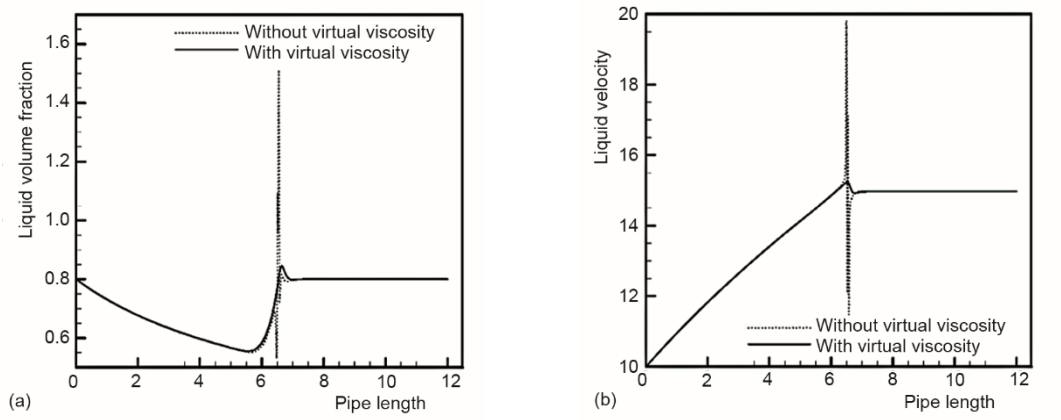

Figure 7. Water faucet problem (CFL = 0.5, computational time = 0.5 seconds); comparison of presence and absence of virtual viscosity for (a) liquid volume fraction and (b) liquid velocity [ms^{-1}] (CFL = 0.5, time = 0.5 seconds, cells = 850)

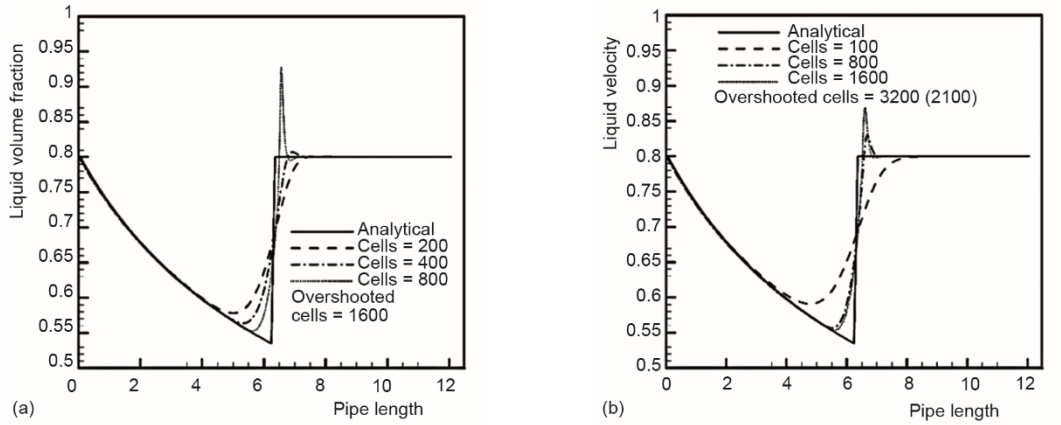

Figure 8. Water faucet problem (CFL = 0.5, computational time = 0.5 seconds); mesh independence study for liquid volume fraction; (a) without virtual viscosity and (b) with virtual viscosity

Conclusions

It has been demonstrated that achieving the grid-independent solutions is very important in any numerical simulation. In this work, an algorithm for water faucet problem which is a famous problem in multiphase flows was developed and implemented in FORTRAN code. Results indicate that Force method is the most appropriate method for simulating this benchmark case but the use of fine meshes would lead to the growth of non-physical instabilities. The ill-posedness of the original model emanates from the extrapolation

of the long wavelength assumption into the short wavelength domain. Short wavelength perturbations induce unbounded growth rates and make it impossible to achieve converging numerical solutions. The approach taken in this article has been to adding virtual viscosity as a CFD technique, is used to remedy this deficiency. Diagrams of liquid velocity and liquid volume fraction are compared for two conditions: with and without virtual viscosity. Results show that wavelengths below the specified cut-off are stabilized and converging solutions are achieved for flow conditions which were ill-posed without adding the virtual viscosity.

References

[1] Bratland, O., *Pipe Flow 2: Multi-phase Flow Assurance*, Dr Ove Bratland Systems Pte. Ltd., Singapore, 2013
[2] Shokri, V., Esmaeili, K., Effect of Liquid Phase Compressibility on Modeling of Gas-Liquid Two-Phase Flows Using Two-Fluid Model, *Thermal Science*, *23* (2019), 5, pp. 3003-3013
[3] Bertola, V., *Modelling and Experimentation in Two-Phase Flow*, Springer-Verlag, Wien, 2003
[4] Ansari, M., Daramizadeh, A., Slug Type Hydrodynamic Instability Analysis Using a Five Equations Hyperbolic Two-Pressure, Two-Fluid Model, *Ocean Engineering*, *52* (2012), Oct., pp. 1-12
[5] Yadigaroglu, G., Hewitt, G., *Introduction to Multiphase Flow*, Springer International Publishing, New York, USA, 2017
[6] Shokri, V., Esmaeili, K., Comparison of the Effect of Hydrodynamic and Hydrostatic Models for Pressure Correction Term in Two-Fluid Model in Gas-Liquid Two-Phase Flow Modelling, *Journal of Molecular Liquids*, *237* (2017), July, pp. 334-346
[7] Essama, O. C., Numerical Modelling of Transient Gas-liquid Flows (Application to Stratified & Slug Flow Regimes), Ph. D. thesis, Department of Applied Mathematics and Computing Group, Cranfield University, Cranfield, UK, 2004
[8] Bahramian, A., Elyasi, S., One-Dimensional Drift-Flux Model and a New Approach to Calculate Drift Velocity and Gas Holdup in Bubble Columns, *Chemical Engineering Science*, *211* (2020), 115302
[9] Bertodano, M., *et al*., *Two Fluid Model Stability Simulation and Chaos*, Springer International Publishing, New York, USA, 2017
[10] Ishii, M., Mishima, K., Two-Fluid Model and Hydrodynamic Constitutive Relations, *Nuclear Engineering and Design*, *82* (1984), 2, pp. 107-126
[11] Issa, R., Kempf, M., Simulation of Slug Flow in Horizontal and Nearly Horizontal Pipes with the Two-Fluid Model, *International journal of multiphase flow*, *29* (2003), 1, pp. 69-95
[12] Jones, V., Prosperetti, A. On the Suitability of First-Order Differential Models for Two-Phase Flow Prediction, *International Journal of Multiphase Flow*, *11* (1985), 2, pp. 133-148
[13] Watson, M., Non-Linear Waves in Pipeline Two-phase Flows, *Proceeding*, 3rd International Conference on Hyperbolic Problems, Uppsala, Sweden, 1990, pp. 11-15
[14] Ransom, V., Hicks, D., Hyperbolic Two-Pressure Models for Two-Phase Flow, *Journal of Computational Physics*, 53 (1984), 1, pp. 124-151
[15] Saurel, R., Abgrall, R. A., Multiphase Godunov Method for Compressible Multifluid and Multiphase Flows, *Journal of Computational Physics*, *150* (1999), 2, pp. 425-467
[16] Wallis, G. B., *One-Dimensional Two-Phase Flow*, McGraw-Hill, New York, USA, 1969
[17] Zolfaghary, A., H., *et al*., The Impact of the Order of Numerical Schemes on Slug Flows Modeling, *Thermal Science*, *23* (2019), 6, pp. 3855-3864
[18] Zolfaghary, A. H., *et al*., Comparison of the Hyperbolic Range of Two-Fluid Models on Two-Phase Gas -Liquid Flows, *International Journal of Engineering*, *31* (2018), 1, pp. 144-156
[19] Barnea, D., Taitel, Y., Interfacial and Structural Stability of Separated Flow, *International Journal of Multiphase Flow*, *20* (1994), 1, pp. 387-414
[20] Mouallem, J., *et al*., Some Accuracy Related Aspects in Two-Fluid Hydrodynamic Sub-Grid Modeling of Gas-Solid Riser Flows, *AIChE Journal*, 66 (2019), 1, e16763
[21] Ansari, M., Shokri, V., Numerical Modeling of Slug Flow Initiation in a Horizontal Channels using a Two-fluid Model, *International Journal of Heat and Fluid Flow*, *32* (2011), 1, pp. 145-155
[22] Montini, M., Closure Relations of the One-Dimensional Two-Fluid Model for the Simulation of Slug Flows, Ph. D. Thesis, Department of Mechanical Engineering, Imperial College London, UK, 2011
[23] White, F., *Viscous Fluid Flow*, 3rd ed., McGraw-Hill Education, New York, USA, 2005

[24] Conte, M. G., *et al*., A Two-Fluid Model for Slug Flow Initiation Based on a Lagrangian Scheme, *Proceeding*, American Society of Mechanical Engineers, Chicago, Ill., USA, 2014, pp. V002T20A003-V002T20A003
[25] Taitel, Y., Dukler, A., A Model for Predicting Flow Regime Transitions in Horizontal and Near Horizontal Gas-Liquid Flow, *AICHE Journal, 22* (1976), 1, pp. 47-55
[26] Woodburn, P. J., Issa, R. J., Well-Posedness of One-Dimensional Transient, Two-Fluid Models of Two-Phase Flows, *Proceedings*, 3rd International Symposium on Mulitphase Flow, ASME Fluids Engineering Division Summer Meeting, Washington, USA, 1998
[27] Anderson, J. D, *Computational Fluid Dynamics: The Basics with Applications*, McGraw-Hill, New York, USA, 1995
[28] Hoffmann, K., Chiang, S., *Computational Fluid Dynamics*, Publication of Engineering Education System,Wichita, Kans., USA, 2000
[29] Pletcher, R., *et al.*, *Computational Fluid Mechanics and Heat Transfer*, Taylor & Francis Group, Oxford, UK, 2013
[30] Toro, E., *Riemann Solvers and Numerical Methods for Fluid Dynamics: A Practical Introduction*, Springer International Publishing, New York, USA, 2009
[31] Hirsch, H., Numerical Computation of Internal and External Flows, in: *Computational Methods for Inviscid and Viscous Flows*, Wiley, New York, USA, 1990, Vol. 2, pp. 536-556
[32] Glowinski, R., *et al*., *Splitting Methods in Communication, Imaging, Science, and Engineering*, Springer International Publishing, New York, USA, 2016
[33] Leveque, R. J., *Finite Volume Methods for Hyperbolic Problems*, Cambridge University Press, Cambridge, UK, 2002
[34] Evje, S., Flatten, T., Hybrid Central-Upwind Schemes for Numerical Resolution of Twophase Flows, *ESAIM: Mathematical Modelling and Numerical Analysis*, *39* (2005), 2, pp. 253-273

Paper submitted: August 1, 2020
Paper revised: February 20, 2021
Paper accepted: February 24, 2021